



Article

Transport Property and Spin–Orbit Torque in 2D Rashba Ferromagnetic Electron Gas

Chao Yang ^{1,*} , Da-Kun Zhou ² , Ya-Ru Wang ² and Zheng-Chuan Wang ^{2,*}¹ College of Mechanical and Electrical Engineering, Wuyi University, Wuyishan 354300, China² School of Physical Sciences, University of Chinese Academy of Sciences, Beijing 100049, China; zhoudakun17@mails.ucas.edu.cn (D.-K.Z.); wangyaru18@mails.ucas.edu.cn (Y.-R.W.)

* Correspondence: wyxy_cyang@163.com (C.Y.); wangzc@ucas.ac.cn (Z.-C.W.)

Abstract: In this paper, we investigate the spin–orbit torque and transport property in a 2D Rashba ferromagnetic electron gas. The longitudinal conductivity can be divided into two parts: the first term is determined by the charge density and is independent of the spin degrees of freedom. The second term depends on the two bands that spin in the opposite directions, and it is directly proportional to spin–orbit torque regardless of the band structure and temperature. This is a general and underlying relation between the transport property and spin–orbit torque. Moreover, we show the impacts of the spin–orbit coupling constant and Fermi energy on transverse conductivity and spin–orbit torque, which is helpful for relevant experiments.

Keywords: 2D Rashba ferromagnetic electron gas; spin-orbit torque; longitudinal conductivity

PACS: 72.25.-b; 75.25.-j; 75.76.+j; 85.75.-d



Citation: Yang, C.; Zhou, D.-K.; Wang, Y.-R.; Wang, Z.-C. Transport Property and Spin–Orbit Torque in 2D Rashba Ferromagnetic Electron Gas. *Materials* **2022**, *15*, 5149. <https://doi.org/10.3390/ma15155149>

Academic Editor: George Kioseoglou

Received: 8 June 2022

Accepted: 19 July 2022

Published: 25 July 2022

Publisher's Note: MDPI stays neutral with regard to jurisdictional claims in published maps and institutional affiliations.



Copyright: © 2022 by the authors. Licensee MDPI, Basel, Switzerland. This article is an open access article distributed under the terms and conditions of the Creative Commons Attribution (CC BY) license (<https://creativecommons.org/licenses/by/4.0/>).

1. Introduction

In recent years, spin–orbit torque has become one of the most attractive topics in the field of spintronics because of its great application prospects in magnetic information storage technology [1–3]. spin–orbit torque (SOT) is based on spin–orbit interaction (SOI), which uses the non-equilibrium spin accumulation induced by charge flow to generate a torque on a local magnetic moment [4,5], thus achieving the purpose of regulating magnetic storage units. SOT-based magnetic random access memory (SOT-MRAM) overcomes the disadvantages of STT-MRAM, especially the fact that it separates the read and write paths, so it has a higher read and write speed and lower power consumption than STT-MRAM [6,7]. Relevant studies show that SOT-MRAM can achieve ultra-fast information writing, which is reduced from the tens of nanoseconds required by the original STT-MRAM to less than 10 ns, while the power consumption of the device is further reduced [8,9].

The essence of spin–orbit torque is that the directional movement of electrons produces a non-equilibrium spin accumulation in the spin–orbit coupling system, by means of the s–d interaction, the spin accumulation of conducting electrons applies a torque on the local magnetic moment [10,11]. Meanwhile, this directional movement of electrons also generates a charge current in general. Thus, the current and spin–orbit torque are both manifestations of the non-equilibrium transport properties of the SOC system, there must be some relations between them. Literature have showed that the magnitude of spin–orbit torque is often proportional to the current density [12–15]. Because the spin accumulation and charge current are proportional to the external electric field under linear transport conditions, the ratio depends on the band structure of the system [4,5]. There is no clear conclusion about the underlying relationship between spin–orbit torque and conductivity.

Two-dimensional Rashba ferromagnetic electron gas is an ideal platform for investigating spin–orbit torque [16,17], and the latter is often realized at heavy metal/ferromagnetic

interfaces [18,19]. These systems have both Rashba spin–orbit interaction and ferromagnetism, and interesting transport phenomena such as spin–orbit torque and anomalous Hall effect have been found [20,21]. In this paper, we use 2D Rashba ferromagnetic electron gas as an example to explore the relationship between spin–orbit torque and transport properties, as well as the regulation of spin–orbit torque. In Section 2, we show the energy splitting caused by spin–orbital interactions; in Section 3, we study the transport properties of the system, including longitudinal conductance and intrinsic anomalous Hall conductivity; in Section 4, we investigate the spin–orbit torque, and show its regulation in terms of the spin–orbit coupling constant and Fermi energy; Section 5 is the conclusion.

2. Model

The Hamiltonian of an electron in a 2D Rashba ferromagnetic electron gas is $\hat{H} = \frac{\hbar^2 \vec{k}^2}{2\mu} + \alpha(\vec{k} \times \vec{z}) \cdot \hat{\sigma} - J\vec{M} \cdot \hat{\sigma}$, where μ is the effective mass of the electron, \vec{M} is the direction of magnetization and we take an out-of-plane magnetization as: $\vec{M} = (0, 0, 1)$, J and α are the constant of the s–d interaction and Rashba spin–orbit coupling. To be sure, the s–d interaction is generated between the electron gas (s electrons) and the local magnetic moments (d electrons), where the latter form a three-dimensional ferromagnetic layer [4,5]. Therefore, the Hamiltonian can be written as [16,17,21]:

$$\hat{H} = \begin{pmatrix} \frac{\hbar^2 k^2}{2\mu} - J & \alpha k_y + i\alpha k_x \\ \alpha k_y - i\alpha k_x & \frac{\hbar^2 k^2}{2\mu} + J \end{pmatrix} \tag{1}$$

Solving the Schrodinger’s equation, we obtain

$$\epsilon_{\uparrow,\downarrow}(\vec{k}) = \frac{\hbar^2 k^2}{2\mu} \pm \sqrt{J^2 + \alpha^2 k^2}, \tag{2}$$

where $\Delta = \sqrt{J^2 + \alpha^2 k^2}$ is the energy splitting of these two bands. Correspondingly, the wavefunctions are $\psi_{\uparrow,\downarrow}(\vec{k}) = e^{i\vec{k} \cdot \vec{r}} |\uparrow, \downarrow\rangle_{\vec{k}}$, where

$$|\uparrow, \downarrow\rangle_{\vec{k}} = \frac{1}{\sqrt{(J \pm \Delta)^2 + \alpha^2 k^2}} \begin{pmatrix} \alpha k_y + i\alpha k_x \\ J \pm \Delta \end{pmatrix}. \tag{3}$$

Then, the average spin of the state $|\uparrow\rangle_{\vec{k}}$ is $\vec{s}(\vec{k}) = \langle \uparrow | \hat{\sigma} | \uparrow \rangle_{\vec{k}} = (\frac{\alpha k_y}{\Delta}, \frac{-\alpha k_x}{\Delta}, \frac{J}{\Delta})$, and the average spin of the state $|\downarrow\rangle_{\vec{k}}$ is $\vec{s}(\vec{k}) = \langle \downarrow | \hat{\sigma} | \downarrow \rangle_{\vec{k}} = -\vec{s}(\vec{k})$.

Figure 1 shows the bands splitting caused by spin–orbit interaction. The spins of electrons in these two bands are in opposite directions, and the energy difference is 2Δ . The band structure depends on the relative magnitudes of α and J . If $\alpha k_J < J$, where $k_J = \sqrt{2\mu J}/\hbar$, ϵ_{\uparrow} and ϵ_{\downarrow} are both parabolic. If $\alpha k_J > J$, ϵ_{\downarrow} has a maximum at $k = 0$ and two bottoms. The specific band structures will affect transport property.

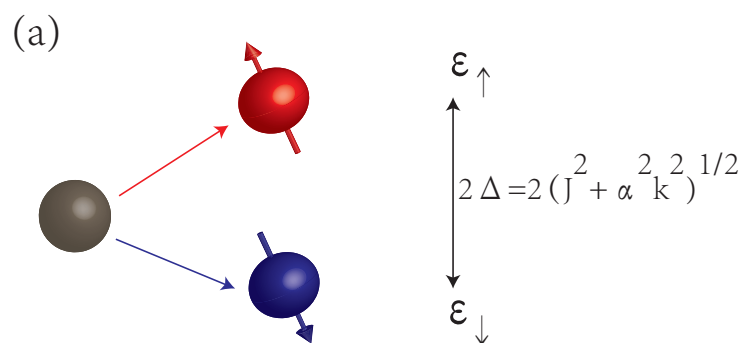


Figure 1. Cont.

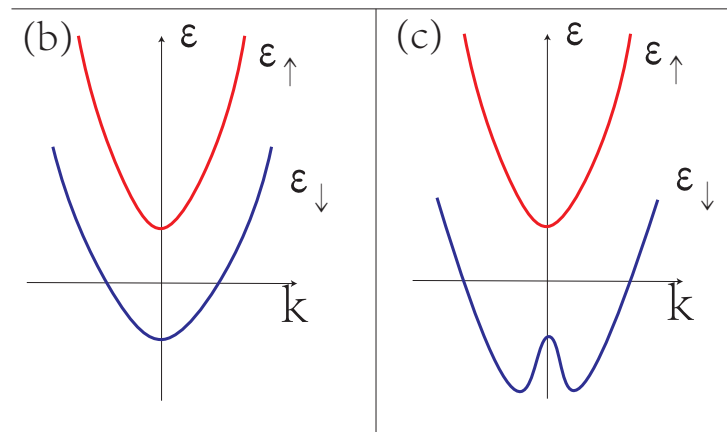


Figure 1. (a) Bands splitting with opposite spins; and bands diagram when (b) $ak_J < J$, (c) $ak_J > J$.

3. Transport Property

In a semiclassical transport equation, the velocity of electrons in band n can be expressed as $v_n = \frac{1}{\hbar} \frac{\partial \epsilon_{kn}}{\partial k} - \frac{e\vec{E}}{\hbar} \times \vec{\Omega}_{kn}$, where $\frac{1}{\hbar} \frac{\partial \epsilon_{kn}}{\partial k}$ is the traditional velocity and $-\frac{e\vec{E}}{\hbar} \times \vec{\Omega}_{kn}$ is the anomalous velocity arising from Berry curvature [22]. In our system, the band splits into $\epsilon_{\uparrow,\downarrow}$, therefore the velocities of electrons are:

$$\vec{v}_{\uparrow,\downarrow} = \frac{1}{\hbar} \vec{\nabla}_k \epsilon_{\uparrow,\downarrow} - \frac{e\vec{E}}{\hbar} \times \vec{\Omega}_{\uparrow,\downarrow} \tag{4}$$

where \vec{E} is the external electric field and the Berry curvature [22] $\vec{\Omega}_{\uparrow,\downarrow}$ can be calculated from wavefunctions: $\vec{\Omega}_{\uparrow,\downarrow}(\vec{k}) = \pm \frac{J\alpha^2}{2\Delta^3} \vec{z}$.

In a weak external electric field, the distribution functions are $f_{\uparrow,\downarrow} = f_{\uparrow,\downarrow}^0 + f_{\uparrow,\downarrow}^1$, where $f_{\uparrow,\downarrow}^0$ are the equilibrium distribution functions, and $f_{\uparrow,\downarrow}^1$ is the first-order perturbation caused by an external electric field. By the relaxation time approximation, $f_{\uparrow,\downarrow}^1$ can be expressed as: $\frac{e\tau}{\hbar} \vec{E} \cdot \vec{\nabla}_k f_{\uparrow,\downarrow}^0$ and τ is the momentum relaxation time [4]. By the definition of current density $\vec{j} = e \int (\vec{v}_{\uparrow} f_{\uparrow} + \vec{v}_{\downarrow} f_{\downarrow}) d\vec{k}$, longitudinal and transverse current densities are:

$$j_x = \frac{e\hbar}{\mu} \int k_x (f_{\uparrow}^1 + f_{\downarrow}^1) d\vec{k} + \frac{e\alpha^2}{\hbar} \int \frac{k_x}{\Delta} (f_{\uparrow}^1 - f_{\downarrow}^1) d\vec{k}, \tag{5}$$

and

$$j_y = \frac{J\alpha^2 e^2 E}{2\hbar} \int \frac{1}{\Delta^3} (f_{\uparrow}^0 - f_{\downarrow}^0) d\vec{k}. \tag{6}$$

To simplify matters, the equilibrium distribution functions can be expressed via the step function at 0K: $f_{\uparrow,\downarrow}^0 = \theta(\epsilon_F - \epsilon_{\uparrow,\downarrow})$, where ϵ_F is the Fermi energy. Thus, the longitudinal conductivity is

$$\sigma_{xx} = \frac{e^2 \tau}{\mu} \int k_x^2 \left(\frac{\partial f_{\uparrow}^0}{\partial k_x} + \frac{\partial f_{\downarrow}^0}{\partial k_x} \right) + \frac{e^2 \alpha^2 \tau}{\hbar^2} \int \frac{k_x^2}{\Delta} \left(\frac{\partial f_{\uparrow}^0}{\partial k_x} - \frac{\partial f_{\downarrow}^0}{\partial k_x} \right), \tag{7}$$

where the first term of Equation (7) can be calculated as:

$$\begin{aligned} \sigma_{xx}^1 &= \frac{e^2 \tau}{\mu} \int k_x^2 \left(\frac{\partial f_{\uparrow}^0}{\partial k_x} + \frac{\partial f_{\downarrow}^0}{\partial k_x} \right) d\vec{k} \\ &= \frac{\pi e^2 \tau}{\mu} (k_{F\uparrow}^2 + k_{F\downarrow}^2), \end{aligned} \tag{8}$$

where $k_{F\uparrow,\downarrow}$ is calculated with the formulas: $\frac{\hbar^2 k^2}{2\mu} \pm \sqrt{J^2 + \alpha^2 k^2} = \epsilon_F$. Allowing for the charge density $n = \int (f_{\uparrow}^0 + f_{\downarrow}^0) = \pi(k_{F\uparrow}^2 + k_{F\downarrow}^2)$, σ_{xx}^1 can be expressed as $\frac{ne^2\tau}{\mu}$ which has the same form with the conductivity of free electron gas. This conductivity is determined by the charge density of electrons, and independent of the spin degree of freedom.

The second term of Equation (7) is derived from the different velocities in two bands:

$$\sigma_{xx}^2 = \frac{e^2\alpha^2\tau}{\hbar^2} \int \frac{k_x^2}{\Delta} \left(\frac{\partial f_{\uparrow}^0}{\partial k_x} - \frac{\partial f_{\downarrow}^0}{\partial k_x} \right) d\vec{k}. \tag{9}$$

This conductivity results from the different velocities of spin-up and spin-down electrons, and reveals the spin-polarized transport property. Considering the change in Fermi surface, we discuss the results in categories:

When $\epsilon_F > J$, the results of equations $\frac{\hbar^2 k^2}{2\mu} \pm \sqrt{J^2 + \alpha^2 k^2} = \epsilon_F$ are $k_{F\uparrow}$ and $k_{F\downarrow}$, respectively. Thus,

$$\sigma_{xx}^2 = \frac{\pi e^2 \alpha^2 \tau}{\hbar^2} \left(\frac{k_{F\downarrow}^2}{\sqrt{J^2 + \alpha^2 k_{F\downarrow}^2}} - \frac{k_{F\uparrow}^2}{\sqrt{J^2 + \alpha^2 k_{F\uparrow}^2}} \right). \tag{10}$$

When $-J < \epsilon_F < J$, the result of equation $\frac{\hbar^2 k^2}{2\mu} - \sqrt{J^2 + \alpha^2 k^2} = \epsilon_F$ is $k_{F\downarrow}$. Thus,

$$\sigma_{xx}^2 = \frac{\pi e^2 \alpha^2 \tau}{\hbar^2} \frac{k_{F\downarrow}^2}{\sqrt{J^2 + \alpha^2 k_{F\downarrow}^2}}. \tag{11}$$

When $\epsilon_F < -J$, only if $\alpha k_j > J$, the equation $\frac{\hbar^2 k^2}{2\mu} - \sqrt{J^2 + \alpha^2 k^2} = \epsilon_F$ has the solutions $k_{F\downarrow 1}$ and $k_{F\downarrow 2}$ ($k_{F\downarrow 1} > k_{F\downarrow 2}$). Thus,

$$\sigma_{xx}^2 = \frac{\pi e^2 \alpha^2 \tau}{\hbar^2} \left(\frac{k_{F\downarrow 1}^2}{\sqrt{J^2 + \alpha^2 k_{F\downarrow 1}^2}} - \frac{k_{F\downarrow 2}^2}{\sqrt{J^2 + \alpha^2 k_{F\downarrow 2}^2}} \right). \tag{12}$$

Figure 2 shows the longitudinal conductivity as a function of Fermi energy ϵ_F . With the increase in ϵ_F , the charge density n increases gradually. Thus, σ_{xx}^1 increases monotonously. At $\epsilon_F = \pm 1$, the number of crossover points of the Fermi surface changes. When $\epsilon_F = -1$, the Fermi surface intersects with the top of ϵ_{\downarrow} at $k = 0$. Below this point, there are two Fermi wave vectors $k_{F\downarrow 1}$ and $k_{F\downarrow 2}$; above that point, σ_{xx}^2 increases with the only Fermi wave vector $k_{F\downarrow}$. Furthermore, when $\epsilon_F = 1$, the Fermi-surface intersects with the bottom of ϵ_{\uparrow} . Above this point, electrons in band ϵ_{\uparrow} participate in the conduction process. From Equation (7), we can see a negative contribution made by ϵ_{\uparrow} . Thus, σ_{xx}^2 decreases gradually.

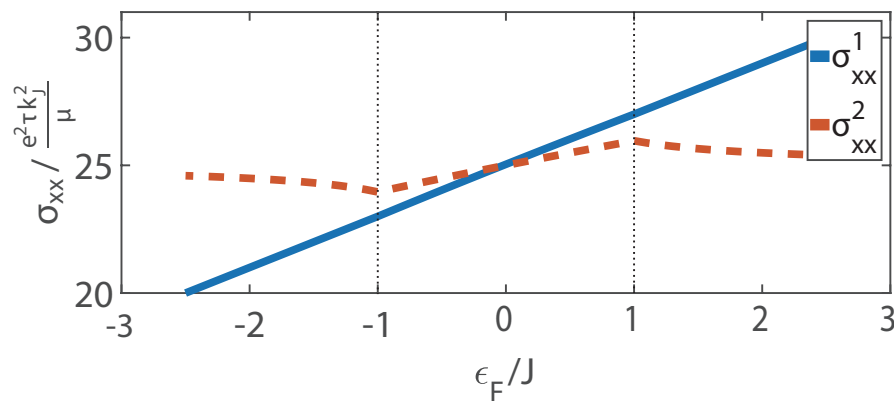


Figure 2. Longitudinal conductivities σ_{xx}^1 and σ_{xx}^2 vs. the Fermi energy ϵ_F , where $\alpha k_j / J = 5$, the solid line is σ_{xx}^1 , and the dashed line is σ_{xx}^2 .

The transverse conductivity is just the intrinsic anomalous Hall conductance, which originates from the Berry curvature [17]. Accordingly, the transverse conductance is

$$\sigma_{xy} = \begin{cases} \frac{\pi J e^2}{2\hbar} \left(\frac{1}{\sqrt{J^2 + \alpha^2 k_{F\downarrow}^2}} - \frac{1}{\sqrt{J^2 + \alpha^2 k_{F\uparrow}^2}} \right) & \epsilon_F > J \\ \frac{\pi J e^2}{2\hbar} \frac{1}{\sqrt{J^2 + \alpha^2 k_{F\downarrow}^2}} & -J < \epsilon_F < J \\ \frac{\pi J e^2}{2\hbar} \left(\frac{1}{\sqrt{J^2 + \alpha^2 k_{F\downarrow 1}^2}} - \frac{1}{\sqrt{J^2 + \alpha^2 k_{F\uparrow 2}^2}} \right) & \epsilon_F > J \end{cases} \quad (13)$$

Figure 3 shows the transverse conductivity as a function of Fermi energy ϵ_F for different band structures. According to Equation (6), σ_{xy} depends on the equilibrium distribution functions $f_{\uparrow,\downarrow}^0$, which means that all states below Fermi energy contribute to transverse conductivity. For $\alpha k_J < J$, ϵ_{\uparrow} and ϵ_{\downarrow} are both parabolic. When $\epsilon_F > J$, ϵ_{\uparrow} begins to make a negative contribution, and thus σ_{xy} decreases. For $\alpha k_J > J$, ϵ_{\downarrow} has a top at $k = 0$ and two bottoms. The maximum of Berry curvature is just at $k = 0$, which means a maximum of transverse velocity. Therefore, the transverse conductivity mainly depends on the states around $k = 0$. When $\epsilon_F < -J$, σ_{xy} increases with the increase in ϵ_F , because the states in ϵ_{\downarrow} around $k = 0$ gradually contribute to σ_{xy} . When $-J < \epsilon_F < J$, σ_{xy} is almost unchanged. When $\epsilon_F > J$, σ_{xy} decreases because of the negative contribution by states in ϵ_{\uparrow} .

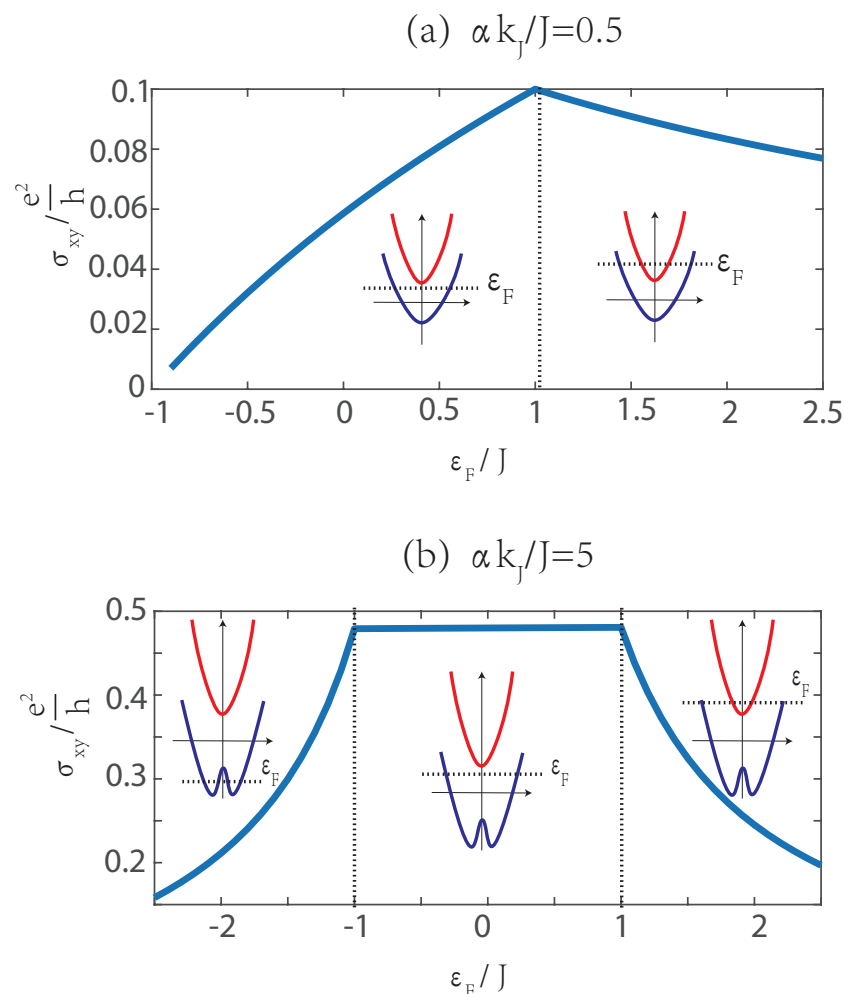


Figure 3. Transverse conductivity σ_{xy} vs. the Fermi energy ϵ_F , where (a) $\alpha k_J / J = 0.5$ and (b) $\alpha k_J / J = 5$, the red line and blue line are bandstructures of ϵ_{\uparrow} and ϵ_{\downarrow} respectively.

4. Spin–Orbit Torque

The spin–orbit torque is the result of s–d interaction between the local magnetic moment and spin accumulation of conduction electrons, and it is always expressed as [23,24]:

$$\vec{T} = -\frac{J}{\hbar} \vec{M} \times \vec{m}, \quad (14)$$

where \vec{m} is the spin accumulation and can be calculated by definition [4,15]:

$$\vec{m} = \hbar \int [\vec{s}(\vec{k}) f_{\uparrow} - \vec{s}(\vec{k}) f_{\downarrow}] d\vec{k}. \quad (15)$$

According to the distribution function above, the spin accumulation along the y axis is

$$m_y = eE\tau\alpha \int \frac{k_x^2}{\Delta} \left(\frac{\partial f_{\uparrow}^0}{\partial k_x} - \frac{\partial f_{\downarrow}^0}{\partial k_x} \right) d\vec{k}. \quad (16)$$

Compared to Equation (9), m_y is directly proportional to σ_{xx}^2 . $m_y/\sigma_{xx}^2 = \hbar^2 E/\epsilon\alpha$, and this specific value is a constant which has no connection with the band structure and temperature. Thus, the spin accumulation m_y and σ_{xx}^2 have the same variation trend in terms of ϵ_F .

Figure 4 shows the spin accumulation m_y as a function of the Rashba SOC constant α . When α is small, the band structure is still parabolic. Therefore, researchers usually treat the spin–orbit interaction as a perturbation [4,5,25]. The interaction between conduction electrons and the local magnetic moment can be regarded as a spin–orbit effective field acting on local magnetic moment [17,26]: $\vec{H}_R = \alpha \langle \vec{k} \rangle \times \vec{z}$, where $\langle \vec{k} \rangle$ is the drift of \vec{k} in an external electric field. $\langle \vec{k} \rangle$ is calculated based on the ferromagnetic electron gas model regardless of the band splitting caused by spin–orbit interaction. Consequently, the spin–orbit torque is a direct proportional function of α . When α is large, $\langle \vec{k} \rangle$ is smaller than the result based on the ferromagnetic electron gas model. Our numerical results show the deviation from the proportional relation.

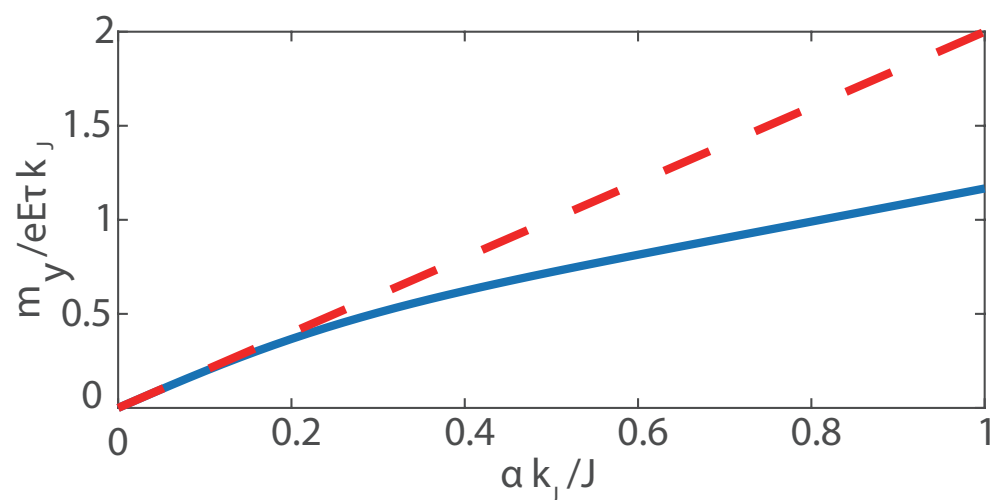


Figure 4. Spin accumulation along the y axis m_y vs. Rashba SOC constant α , where the solid line is the result based on the split bands and the dashed line is based on the band of ferromagnetic electron gas.

Similarly, the spin accumulation along the z axis is

$$m_z = \hbar \int [s_z(\vec{k})(f_{\uparrow}^0 - f_{\downarrow}^0)] d\vec{k}. \quad (17)$$

This spin accumulation depends on the equilibrium distribution function and is parallel to the local magnetic moment; thus, it makes no contribution to the spin–orbit torque.

5. Conclusions

In this paper, we investigated the spin–orbit torque and transport property in a 2D Rashba ferromagnet. The main conclusions are as follows:

The longitudinal conductivity can be divided into two parts: the first term is determined by the charge density and is independent of the spin degrees of freedom. The second term depends on the two bands that spin in opposite directions, and this reflects the spin-polarized transport property of the system.

The spin–orbit torque is directly proportional to the second term of longitudinal conductivity, because spin–orbit torque is just caused by the spin-polarized transport. Although this conclusion is obtained at 0K and using parabolic bands, it is suitable for general linear transport cases. This proportionate relation reveals the underlying connection between spin–orbit torque and conductivity.

Moreover, we demonstrate the impacts of the spin–orbit coupling constant and Fermi energy on spin–orbit torque. When these constants are experimentally changed, the spin–orbit torque can be adjusted accordingly. The results are helpful for relevant experiments.

Author Contributions: Conceptualization, C.Y. and Z.-C.W.; Data curation, C.Y.; Formal analysis, C.Y., D.-K.Z. and Y.-R.W.; Investigation, C.Y., D.-K.Z. and Z.-C.W.; Methodology, D.-K.Z. and Z.-C.W.; Writing—original draft, C.Y.; Writing—review & editing, D.-K.Z., Y.-R.W. and Z.-C.W. All authors have read and agreed to the published version of the manuscript.

Funding: This research was funded by the Natural Science Foundation of Fujian Province, China (Grant No. 2021J05245) and Wuyi University (Grant No. YJ202014). The APC was funded by the Natural Science Foundation of Fujian Province, China (Grant No. 2021J05245).

Data Availability Statement: The data that support the results of this research are available from the corresponding author, [C.Y], upon reasonable request.

Conflicts of Interest: The authors declare no conflict of interest.

References

1. Manchon, A. A new moment for Berry. *Nat. Phys.* **2014**, *10*, 340–341. [[CrossRef](#)]
2. Kuschel, T.; Reiss, G. Charges ride the spin wave. *Nat. Nanotechnol.* **2014**, *10*, 22–24. [[CrossRef](#)] [[PubMed](#)]
3. Molavi, M.; Faizabadi, E. Spin-polarization and spin-flip in a triple-quantum-dot ring by using tunable lateral bias voltage and Rashba spin-orbit interaction. *J. Magn. Magn. Mater.* **2017**, *428*, 488–492. [[CrossRef](#)]
4. Manchon, A.; Zhang, S. Theory of nonequilibrium intrinsic spin torque in a single nanomagnet. *Phys. Rev. B* **2008**, *78*, 212405. [[CrossRef](#)]
5. Manchon, A.; Zhang, S. Theory of spin torque due to spin-orbit coupling. *Phys. Rev. B* **2009**, *79*, 094422. [[CrossRef](#)]
6. Prenat, G.; Jabeur, K.; Pendina, G.D.; Bouille, O.; Gaudin, G. Beyond STT-MRAM, Spin Orbit Torque RAM SOT-MRAM for High Speed and High Reliability Applications. In *Spintronics-Based Computing*; Springer International Publishing: Berlin/Heidelberg, Germany, 2015; pp. 145–157. [[CrossRef](#)]
7. Fukami, S.; Zhang, C.; Duttgupta, S.; Kurenkov, A.; Ohno, H. Magnetization switching by spin–orbit torque in an antiferromagnet–ferromagnet bilayer system. *Nat. Mater.* **2016**, *15*, 535–541. [[CrossRef](#)]
8. Cubukcu, M.; Bouille, O.; Mikuszeit, N.; Hamelin, C.; Bracher, T.; Lamard, N.; Cyrille, M.C.; Buda-Prejbeanu, L.; Garello, K.; Miron, I.M.; et al. Ultra-Fast Perpendicular Spin–Orbit Torque MRAM. *IEEE Trans. Magn.* **2018**, *54*, 1–4. [[CrossRef](#)]
9. Salehi, S.; DeMara, R.F. Adaptive Non-Uniform Compressive Sensing Using SOT-MRAM Multi-Bit Precision Crossbar Arrays. *IEEE Trans. Nanotechnol.* **2021**, *20*, 224–228. [[CrossRef](#)]
10. Chung, N.L.; Jalil, M.B.A.; Tan, S.G. Non-equilibrium spatial distribution of Rashba spin torque in ferromagnetic metal layer. *AIP Adv.* **2012**, *2*, 022165. [[CrossRef](#)]
11. Wang, X.; Pauyac, C.O.; Manchon, A. Spin-orbit-coupled transport and spin torque in a ferromagnetic heterostructure. *Phys. Rev. B* **2014**, *89*, 054405. [[CrossRef](#)]
12. Wang, X.; Manchon, A. Diffusive Spin Dynamics in Ferromagnetic Thin Films with a Rashba Interaction. *Phys. Rev. Lett.* **2012**, *108*, 117201. [[CrossRef](#)] [[PubMed](#)]
13. Brataas, A.; Kent, A.D.; Ohno, H. Current-induced torques in magnetic materials. *Nat. Mater.* **2012**, *11*, 372–381. [[CrossRef](#)] [[PubMed](#)]
14. Hals, K.M.D.; Brataas, A. Phenomenology of current-induced spin-orbit torques. *Phys. Rev. B* **2013**, *88*, 085423. [[CrossRef](#)]

15. Yang, C.; Wang, Z.C.; Zheng, Q.R.; Su, G. Generalized spin-orbit torques in two-dimensional ferromagnets with spin-orbit coupling. *Eur. Phys. J. B* **2019**, *92*, 1–7. [[CrossRef](#)]
16. Jiang, Y.; Jalil, M.B.A. Enhanced spin injection and magnetoconductance by controllable Rashba coupling in a ferromagnet/two-dimensional electron gas structure. *J. Phys. Condens. Matter* **2003**, *15*, L31–L39. [[CrossRef](#)]
17. Ado, I.; Qaiumzadeh, A.; Duine, R.; Brataas, A.; Titov, M. Asymmetric and Symmetric Exchange in a Generalized 2D Rashba Ferromagnet. *Phys. Rev. Lett.* **2018**, *121*, 086802. [[CrossRef](#)]
18. Haney, P.M.; Lee, H.W.; Lee, K.J.; Manchon, A.; Stiles, M.D. Current-induced torques and interfacial spin-orbit coupling. *Phys. Rev. B* **2013**, *88*, 214417. [[CrossRef](#)]
19. Pauyac, C.O.; Chshiev, M.; Manchon, A.; Nikolaev, S.A. Spin Hall and Spin Swapping Torques in Diffusive Ferromagnets. *Phys. Rev. Lett.* **2018**, *120*, 176802. [[CrossRef](#)]
20. Zhang, Z.Y. Charge transport through ferromagnet/two-dimensional electron gas/d-wave superconductor junctions with Rashba spin-orbit coupling. *Eur. Phys. J. B* **2008**, *63*, 65–69. [[CrossRef](#)]
21. Ado, I.; Dmitriev, I.; Ostrovsky, P.; Titov, M. Anomalous Hall Effect in a 2D Rashba Ferromagnet. *Phys. Rev. Lett.* **2016**, *117*, 046601. [[CrossRef](#)]
22. Xiao, D.; Chang, M.C.; Niu, Q. Berry phase effects on electronic properties. *Rev. Mod. Phys.* **2010**, *82*, 1959–2007. [[CrossRef](#)]
23. Matos-Abiague, A.; Rodríguez-Suárez, R.L. Spin-orbit coupling mediated spin torque in a single ferromagnetic layer. *Phys. Rev. B* **2009**, *80*, 094424. [[CrossRef](#)]
24. Li, H.; Wang, X.; Doğan, F.; Manchon, A. Tailoring spin-orbit torque in diluted magnetic semiconductors. *Appl. Phys. Lett.* **2013**, *102*, 192411. [[CrossRef](#)]
25. Pesin, D.A.; MacDonald, A.H. Quantum kinetic theory of current-induced torques in Rashba ferromagnets. *Phys. Rev. B* **2012**, *86*, 014416. [[CrossRef](#)]
26. Chernyshov, A.; Overby, M.; Liu, X.; Furdyna, J.K.; Lyanda-Geller, Y.; Rokhinson, L.P. Evidence for reversible control of magnetization in a ferromagnetic material by means of spin-orbit magnetic field. *Nat. Phys.* **2009**, *5*, 656–659. [[CrossRef](#)]